eNeurologicalSci 23 (2021) 100343

Contents lists available at ScienceDirect

eNeurologicalSci

journal homepage: www.elsevier.com/locate/ensci

Voxel-based correlation of ^{18}F-THK5351 accumulation with gray matter structural networks in cognitively normal older adults

Yoko Shigemoto [a,b], Daichi Sone [c], Norihide Maikusa [c], Yukio Kimura [a], Fumio Suzuki [a], Hiroyuki Fujii [a], Noriko Sato [a], Hiroshi Matsuda [a,b,*]

[a] Department of Radiology, National Center of Neurology and Psychiatry, 4-1-1, Ogawa-Higashi, Kodaira, Tokyo 187-8551, Japan
[b] Cyclotron and Drug Discovery Research Center, Southern TOHOKU Research Institute for Neuroscience, Koriyama, Fukushima 963-8052, Japan
[c] Integrative Brain Imaging Center, National Center of Neurology and Psychiatry, 4-1-1, Ogawa-Higashi, Kodaira, Tokyo 187-8551, Japan

ARTICLE INFO

Keywords:
Caudate nucleus
Cognitively normal older adult
Gray matter
Network
Tau

ABSTRACT

Objective: The aim of this study was to evaluate tau-related structural network metrics derived from gray matter magnetic resonance imaging (MRI) scans in cognitively normal (CN) older adults.
Methods: We recruited 47 amyloid-negative CN older adults (mean age ± standard deviation, 65.0 ± 7.9 years; 26 women). All participants underwent 3D T1-weighted MRI and ^{11}C-Pittsburgh compound-B and ^{18}F-THK5351 positron emission tomography scans. Four local network metrics (betweenness centrality, clustering coefficient, characteristic path length, and degree) were computed and rendered on individual brain images. We then evaluated the correlations between ^{18}F-THK5351 positron emission tomography images and local network metric images at the voxel level.
Results: Significant positive correlations of the four local network metrics with ^{18}F-THK5351 were detected in the bilateral caudate.
Conclusion: Our findings suggest that tau and neuroinflammation in CN older adults may influence the gray matter structural network in the caudate.

1. Introduction

Aging is a complex process that can be a major risk factor for neurodegenerative diseases, including Alzheimer's disease (AD) [1–3]. Normal aging is accompanied by several neuropathological changes, such as neuroinflammation and accumulation of misfolded proteins. Previous neuropathological studies have shown that tau-related neurofibrillary tangles accumulate in the medial temporal lobe (MTL) with aging, even in individuals with normal cognitive function [4].

These age-related changes can now by evaluated in vivo owing to the recent advent of molecular imaging. ^{18}F-THK5351, one of the first-generation tau positron emission tomography (PET) tracers, reveals tau-associated regions in AD and is considered a promising biomarker for tau [5]. However, several studies have clarified that ^{18}F-THK5351 reflects not only tau but also astrogliosis-related neuroinflammation because of off-target binding to monoamine oxidase B (MAO-B) [6]. Therefore, ^{18}F-THK5351 may provide important information on both tau and inflammatory pathology with aging.

The human brain comprises a complex network composed of billions of neurons. Network analysis based on graph theory has provided new insight into the understanding of brain networks using resting-state functional magnetic resonance imaging (fMRI) and diffusion tensor imaging [7,8]. However, these MRI protocols are usually used for research purposes owing to their long acquisition times. Moreover, resting-state fMRI is susceptible to the influence of physiological conditions [9] and diffusion tensor imaging results vary among scanner vendors [10]. To solve these problems, Tijms et al. [11] proposed a new method based on similarities of gray matter (GM) features in individual brains using 3D T1-weighted images, which are obtained in routine clinical practice. They have applied this method to healthy individuals and shown that it can obtain reproducible results that are equivalent to those provided by other modalities [11]. Other studies, including ours, have also applied this method and detected disease-related structural network changes in AD [12], multiple sclerosis [13], bipolar disorder [14], and myalgic encephalomyelitis/chronic fatigue syndrome [15].

We have previously applied this method to healthy individuals to

* Corresponding author at: Cyclotron and Drug Discovery Research Center, Southern TOHOKU Research Institute for Neuroscience, Shin-Otemachi Bulding 6F (621), 2-2-1, Otemachi, Chiyoda-ku, Tokyo 199-0004, Japan.
E-mail address: hiroshi.matsuda@mt.strins.or.jp (H. Matsuda).

https://doi.org/10.1016/j.ensci.2021.100343
Received 10 February 2021; Received in revised form 14 April 2021; Accepted 25 April 2021
Available online 28 April 2021

examine the correlation between local network metrics and cerebral ^{18}F-THK5351 accumulation and found positive correlations in several cerebral regions, including the default mode network area [16]. However, this correlation was observed at the global level of ^{18}F-THK5351 accumulation. A further local correlation study may be necessary for elucidation of the direct influence of tau/inflammatory changes on the structural network. Thus, the purpose of the present study was to investigate the local correlation of ^{18}F-THK5351 accumulation and network metrics by direct comparison at the voxel level.

2. Materials and methods

2.1. Participants

We recruited 47 cognitively normal (CN) older adults from the Brain Mapping by Integrated Neurotechnologies for Disease Studies (Brain/MINDS) project (grant number 18dm0207017h0005). All individuals underwent structural MRI and ^{11}C-Pittsburgh compound-B (^{11}C-PiB) and ^{18}F-THK5351 PET scans, as well as cognitive testing that included the Mini-Mental State Examination (MMSE), global Clinical Dementia Rating Scale (CDR), and Wechsler Memory Scale-Revised Logical Memory II (WMSR LM-II). Inclusion criteria were as follows: visually negative ^{11}C-PiB PET results, a global CDR score of 0, an MMSE score of $\geq$26, performance within education-adjusted norms for the WMSR LM-II, no neurological or psychiatric disorders, and no medications affecting cognition. Amyloid negativity was visually determined by a board-certified nuclear medicine specialist.

All participants provided written informed consent to participate in the study, which was approved by the institutional ethics committee at the National Center of Neurology and Psychiatry, Tokyo (approval A2014-146).

2.2. MRI and PET data acquisition and processing

All participants underwent structural MRI scans on a Siemens 3-T scanner (Verio; Siemens, Erlangen, Germany) to obtain 3D sagittal T1-weighted magnetization-prepared rapid acquisition with gradient echo images (repetition time/echo time, 1.900/2.52 ms; 1.0-mm effective slice thickness with no gap; 300 slices; matrix, 256 × 256; field of view, 25 × 25 cm; acquisition time; 4 min 18 s).

All PET/computed tomography (CT) scans were acquired using a Siemens/Biograph TruePoint16 Scanner (3D acquisition mode; 81 image planes; 16.2-cm axial field of view; 4.2-mm transaxial resolution; 4.7-mm axial resolution; 2-mm slice interval). Low-dose CT scans for attenuation correction were performed prior to the PET scans. ^{11}C-PiB PET scans were acquired as dynamic scans in LIST mode 50–70 min after a bolus injection of 555 ± 185 MBq of ^{11}C-PiB. ^{18}F-THK5351 scans were acquired as dynamic scans in LIST mode 40–60 min after a bolus injection of 185 ± 37 MBq of ^{18}F-THK5351. PET/CT data were reconstructed using an iterative 3D ordered subset expectation maximization reconstruction algorithm. All MRI and PET data were acquired in the same manner as in a previous study [17].

2.3. Postprocessing of MRI and PET data

GM images were segmented from 3D T1-weighted images using Statistical Parametric Mapping Software version 12 (SPM12; Functional Imaging Laboratory, University College London, London, UK). The ^{11}C-PiB and ^{18}F-THK5351 PET data were partial volume-corrected using the SPM toolbox PETPVE12 [18]. Each participant's PET images were then coregistered to the corresponding T1-weighted images and normalized with the Diffeomorphic Anatomical Registration Through Exponentiated Lie (DARTEL) method [19]. After spatial normalization, the standardized uptake value ratios (SUVRs) for PET images were calculated using the individual's positive mean uptake value of cerebellar GM as the reference region. Finally, SUVR of each PET image was smoothed using an 8-mm full width at half maximum (FWHM) Gaussian kernel. MRI and PET data were processed in the same manner as in a previous study [17].

2.4. Single-subject GM networks

We calculated the following local network metrics using the similarity-based method [11]: betweenness centrality (i.e., the proportion of the shortest paths running through a node), clustering coefficient (i.e., the level of interconnectedness of neighboring nodes), characteristic path length (i.e., the shortest distance between two nodes), and degree (i.e., the number of edges per node). These network metric images were rendered on individual brain images as previously described [14–16]. First, we resliced the segmented GM images into 2 × 2 × 2-mm isovoxels. Then, we calculated the network metric images from the segmented GM images in native space. In this network analysis, nodes were defined as small brain areas (regions of 3 × 3 × 3 voxels) and connectivity was based on similarity in the spatial structure of GM density values quantified with Pearson's correlations. The networks were binarized using subject-specific thresholds determined using a random permutation method that ensured the inclusion of at most a 5% chance of spurious correlations in the network [20].

To evaluate network metric images at the voxel level, network images were normalized with DARTEL [19]. Each network metric image was smoothed using a 10-mm FWHM Gaussian kernel in the same manner as in previous studies [14–16].

2.5. Voxel-wise correlations between ^{18}F-THK5351 PET and the GM network

To evaluate correlations between ^{18}F-THK5351 and local network metrics, we used the Biological Parametric Mapping (BPM) toolbox [21]. This toolbox allows voxel-wise correlations across two imaging modalities based on the general linear model. We analyzed the correlations between ^{18}F-THK5351 and four local network metrics (betweenness centrality, clustering coefficient, characteristic path length, and degree). Results with the following criteria were deemed significant: family-wise error-corrected at $p < .05$ and an extent threshold of 100 voxels.

3. Results

Participants' demographics are shown in Table 1. Mean age ± standard deviation was 65.0 ± 7.9 years and 26 of the participants (55%) were women. Mean cognitive scores were 0.0 ± 0.2 for the CDR sum of boxes, 29.3 ± 1.1 for the MMSE, and 13.4 ± 2.9 for the WMSR LM-II.

^{18}F-THK5351 showed cerebral accumulation mainly in the MTL and, to a lesser extent, in the inferior temporal lobe, insula, posterior cingulate/precuneus, and basal frontal lobe (Fig. 1). Elevated ^{18}F-THK5351 accumulation was also observed in the caudate nucleus, putamen, and thalamus.

Significant positive correlations were found between ^{18}F-THK5351 and the four local network metrics in the bilateral caudate (Table 2 and

Table 1
Participants' demographics.

	Cognitively normal older adults
No. (women)	47 (26)
Age, years	65.0 ± 7.9 [50–86]
Education, years	14.3 ± 2.4 [9–22]
MMSE	29.3 ± 1.1 [26–30]
WMSR LM-II	13.4 ± 2.9 [8–19]

Values are the mean ± standard deviation [range]. MMSE, Mini-Mental State Examination; WMSR LM-II, Wechsler Memory Scale-Revised Logical Memory II.

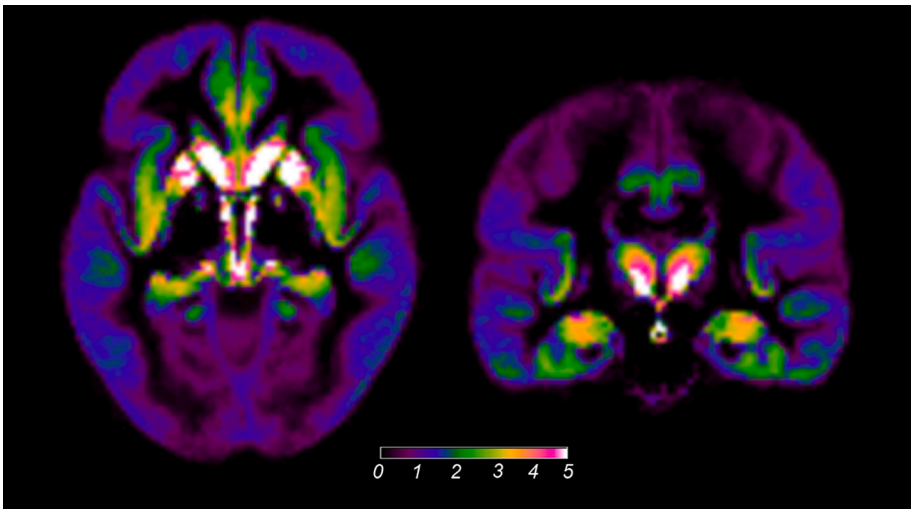

Fig. 1. Mean SUVR images of ^{18}F-THK5351 in cognitively normal older adults. SUVR, standardized uptake value ratio.

Table 2
Clusters of positive correlations between ^{18}F-THK5351 accumulation and local network metrics detected by voxel-wise correlation analysis using biological parametric mapping.

	Cluster size (no. of voxels)	*T*-value (peak voxel)	Talairach coordinates (*x*, *y*, *z*)	Location of peak voxels	
Betweenness centrality	432	Inf	8, 14, 14	Right	Caudate*
Clustering coefficient	313	6.98	−6, 6, 13	Left	Caudate
Characteristic path length	357	7.06	−6, 6, 13	Left	Caudate
Degree	505	7.57	−4, 6, 11	Left	Caudate*

Results were family-wise error-corrected for multiple comparisons ($p < .05$) with an extent threshold of 100 voxels.
* Note that these are the nearest gray matter regions to the peak voxels.

Fig. 2). No significant negative correlations were detected.

4. Discussion

This is the first study to investigate the direct voxel-wise imaging correlations between ^{18}F-THK5351 and local network metrics in amyloid-negative CN older adults. We identified positive correlations of ^{18}F-THK5351 with local GM network metrics in the bilateral caudate. These findings suggest that tau and inflammatory pathology in CN older adults may influence the local GM network in the caudate.

We found cerebral ^{18}F-THK5351 accumulation mainly in the MTL and, to a lesser extent, in the inferior temporal lobe, insula, posterior cingulate/precuneus, and basal frontal lobe. These findings correspond to Braak stage III–IV and are considered to reflect primary age-related tauopathy (PART) [22]. In addition, elevated ^{18}F-THK5351 accumulation was observed in the caudate nucleus, putamen, and thalamus, which was considered to be largely due to non-specific binding to MAO-

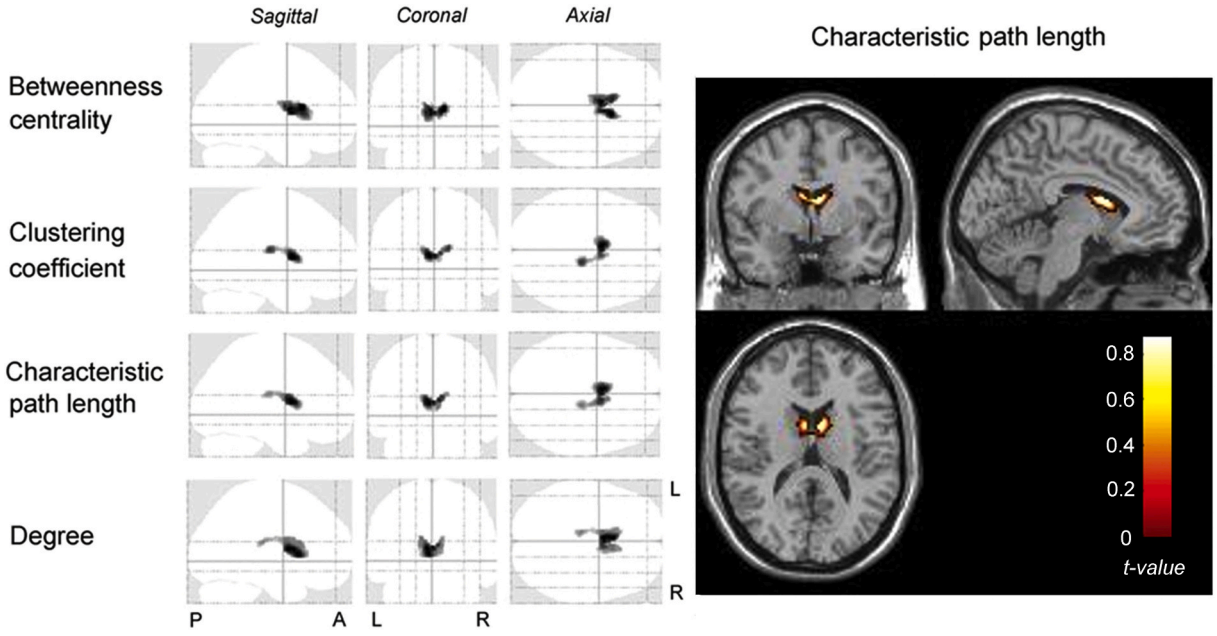

Fig. 2. Voxel-wise correlations between ^{18}F-THK5351 and four local network metrics in cognitively normal older adults. Significant positive correlations between ^{18}F-THK5351 and local network metrics were detected in the bilateral caudate (family-wise error-corrected $p < .05$ with a 100-voxel extent threshold). A, anterior; L, left; P, posterior; R, right.

B [23].

The similarity-based GM network method allows direct comparisons of local network metrics images via the rendering of each metric image in Montreal Neurological Institute space. BPM analysis revealed significant voxel-wise positive correlations of ^{18}F-THK5351 in the caudate with four local network metrics based on graph theory. Betweenness centrality is the proportion of the shortest paths that run through a node and our findings suggest that the caudate plays an important role as a hub. An increased clustering coefficient indicates the progress of segregation with ^{18}F-THK5351 accumulation, whereas an increased characteristic path length suggests a decrease in network integration in the caudate. Thus, although the caudate is overactivated as a hub and in local network segregation progresses, tau and inflammatory pathology also locally disrupt the network integration.

Neuropathological studies have shown that tau pathology accumulates in the caudate nucleus as well as in the MTL in PART patients with higher Braak stages (e.g., III/IV) [24]. In addition, a previous PET study using [^{11}C]L-deprenyl-D2 reported that MAO-B levels in the basal ganglia increase by an average of 8% per decade in healthy individuals [25]. Another study using quantitative enzyme radioautography and in situ hybridization histochemistry also detected high levels of MAO-B in the caudate nucleus [26]. MAO-B levels increase with age and are considered to elevate oxidative stress, which may worsen the vulnerability of the brain dopamine system to age-related degeneration [27]. A recent structural network study using T1-weighted images in patients with idiopathic rapid eye movement sleep behavior disorder, which often precedes neurodegenerative disease, reported overactivity of the caudate nucleus as a hub, suggesting that such overactivity might be a potential biomarker of this sleep behavior disorder [28].

Anatomically, the caudate nucleus is connected to the MTL and is part of the cortico-striato-thalamic loop [29,30]. The caudate plays a critical role in cognitive aging, which includes decreases in the functioning of inhibitory mechanisms, executive control, or planning and cognitive function, as determined by increases in response times [31]. Moreover, the caudate appears to be linked to apathy [32], which is the most frequent abnormal behavior before memory deficits become noticeable in AD. A recent systematic review and meta-analysis reported that apathy was associated with an approximately 2-fold increased risk of dementia in memory clinic patients, indicating that apathy might be one of the useful indicators of prodromal dementia [33]. Several MRI studies have detected reductions in caudate volume with aging [34,35], which is consistent with previous autopsy data indicating an estimated 15% decrease in caudate volume from ages 25 to 75 years [36]. This atrophy may be secondary to the accumulation of tau and inflammatory pathology in the caudate. Because the caudate is connected to the MTL, our findings of both overactivity and local network disruption in the caudate may be induced by tau and neuroinflammation in the MTL, which is the first brain region to be affected by tau pathology with aging.

This study has several limitations. First, this study had a relatively small number of participants. Second, we did not conduct correlation analysis of networks using other modalities such as resting-state functional MRI or diffusion tensor imaging. However, Tijms et al. [11] applied this method to healthy individuals and obtained similar results to those determined using other modalities. Third, we found that some of the peak voxels were contained inside the lateral ventricles adjacent to the caudate. This reduced accuracy of anatomical registration might be caused by the use of large 6-mm cube voxels, which are necessary to maintain the 3D structure of the cortex. Fourth, this study was a cross-sectional design, so we did not know if the disturbance of the network metrics in the caudate has some predictive value in CN older adults. Longitudinal evaluation in the same subjects is needed to support our results. Fifth, no significant correlations were detected between neuropsychological tests and the network changes, which is possibly owing to the small sample size and inclusion of cognitively healthy subjects. We would like to evaluate more detailed cognitive testing such as WAIS-III subscores to reveal subtle neurocognitive changes related to the network changes in the caudate.

5. Conclusions

We found voxel-wise positive correlations between ^{18}F-THK5351 and local network metrics in the caudate. Our results suggest that tau and inflammatory pathology may influence local GM network metrics of the caudate in CN older adults.

Grant support

This study was supported by the following funding sources: the Brain Mapping by Integrated Neurotechnologies for Disease Studies (Brain/MINDS) project (grant no. 18dm0207017h0005), the Japan Agency for Medical Research and Development (AMED), and an Intramural Research Grant (30-10) for Neurological and Psychiatric Disorders from the National Center of Neurology and Psychiatry (Japan).

Declaration of Competing Interest

None.

Acknowledgements

We would like to thank Mr. Tetsuro Ono of Dainippon Printing Co., Ltd., for valuable suggestions regarding network analyses. We also thank all imaging technicians who contributed to the study.

References

[1] A. Bektas, S.H. Schurman, R. Sen, et al., Aging, inflammation and the environment, Exp. Gerontol. 105 (2018) 10–18, https://doi.org/10.1016/j.exger.2017.12.015.
[2] A. Kumar, Editorial: neuroinflammation and cognition, Front. Aging Neurosci. 10 (2018) 413, https://doi.org/10.3389/fnagi.2018.00413.
[3] V. Calsolaro, P. Edison, Neuroinflammation in Alzheimer's disease: current evidence and future directions, Alzheimers Dement. 12 (6) (2016) 719–732, https://doi.org/10.1016/j.jalz.2016.02.010.
[4] H. Braak, D.R. Thal, E. Ghebremedhin, et al., Stages of the pathologic process in Alzheimer disease: age categories from 1 to 100 years, J. Neuropathol. Exp. Neurol. 70 (11) (2011) 960–969, https://doi.org/10.1097/NEN.0b013e318232a379.
[5] T.J. Betthauser, P.J. Lao, D. Murali, et al., In vivo comparison of tau radioligands ^{18}F-THK-5351 and ^{18}F-THK-5317, J. Nucl. Med. 58 (6) (2017) 996–1002, https://doi.org/10.2967/jnumed.116.182980.
[6] N. Okamura, R. Harada, A. Ishiki, et al., The development and validation of tau PET tracers: current status and future directions, Clin. Transl. Imaging 6 (2018) 305–316, https://doi.org/10.1007/s40336-018-0290-y.
[7] E. Bullmore, O. Sporns, Complex brain networks: graph theoretical analysis of structural and functional systems, Nat. Rev. Neurosci. 10 (3) (2009) 186–198, https://doi.org/10.1038/nrn2575.
[8] O. Sporns, G. Tononi, R. Kötter, The human connectome: a structural description of the human brain, PLoS Comput. Biol. 1 (4) (2005), e42, https://doi.org/10.1371/journal.pcbi.0010042.
[9] R.M. Birn, M.D. Cornejo, E.K. Molloy, et al., The influence of physiological noise correction on test–retest reliability of resting-state functional connectivity, Brain Connect. 4 (7) (2014) 511–522, https://doi.org/10.1089/brain.2014.0284.
[10] J. Min, M. Park, J.W. Choi, et al., Inter-vendor and inter-session reliability of diffusion tensor imaging: implications for multicenter clinical imaging studies, Korean J. Radiol. 19 (4) (2018) 777–782, https://doi.org/10.3348/kjr.2018.19.4.777.
[11] B.M. Tijms, P. Seriès, D.J. Willshaw, et al., Similarity-based extraction of individual networks from gray matter MRI scans, Cereb. Cortex 22 (7) (2012) 1530–1541, https://doi.org/10.1093/cercor/bhr221.
[12] B.M. Tijms, C. Möller, H. Vrenken, et al., Single-subject grey matter graphs in Alzheimer's disease, PLoS One 8 (3) (2013), e58921, https://doi.org/10.1371/journal.pone.0058921.
[13] C.M. Rimkus, M.M. Schoonheim, M.D. Steenwijk, et al., Gray matter networks and cognitive impairment in multiple sclerosis, Mult. Scler. 25 (3) (2019) 382–391, https://doi.org/10.1177/1352458517751650.
[14] M. Ota, T. Noda, N. Sato, et al., Structural brain network differences in bipolar disorder using with similarity-based approach, Acta Neuropsychiatr. 22 (2020) 1–5, https://doi.org/10.1017/neu.2020.45.
[15] H. Fujii, W. Sato, Y. Kimura, et al., Altered structural brain networks related to adrenergic/muscarinic receptor autoantibodies in chronic fatigue syndrome, J. Neuroimaging 30 (6) (2020) 822–827, https://doi.org/10.1111/jon.12751.
[16] Y. Shigemoto, D. Sone, K. Okita, et al., Gray matter structural networks related to ^{18}F-THK5351 retention in cognitively normal older adults and Alzheimer's disease

patients, eNeurologicalSci. 22 (4) (2021) 100309, https://doi.org/10.1016/j.ensci.2021.100309.
[17] Y. Shigemoto, D. Sone, E. Imabayashi, et al., Dissociation of tau deposits and brain atrophy in early Alzheimer's disease: a combined positron emission tomography/magnetic resonance imaging study, Front. Aging Neurosci. 10 (2018) 223, https://doi.org/10.3389/fnagi.2018.00223.
[18] G. Gonzalez-Escamilla, C. Lange, S. Teipel, et al., PETPVE12: an SPM toolbox for partial volume effects correction in brain PET - application to amyloid imaging with AV45-PET, Neuroimage. 147 (2017) 669–677, https://doi.org/10.1016/j.neuroimage.2016.12.077.
[19] J. Ashburner, A fast diffeomorphic image registration algorithm, Neuroimage 38 (1) (2007) 95–113, https://doi.org/10.1016/j.neuroimage.2007.07.007.
[20] W.S. Noble, How does multiple testing correction work? Nat. Biotechnol. 27 (2009) 1135–1137, https://doi.org/10.1038/nbt1209-1135.
[21] R. Casanova, R. Srikanth, A. Baer, et al., Biological parametric mapping: a statistical toolbox for multimodality brain image analysis, Neuroimage 34 (1) (2007) 137–143, https://doi.org/10.1016/j.neuroimage.2006.09.011.
[22] J.F. Crary, J.Q. Trojanowski, J.A. Schneider, et al., Primary age-related tauopathy (PART): a common pathology associated with human aging, Acta Neuropathol. 128 (6) (2014) 755–766, https://doi.org/10.1007/s00401-014-1349-0.
[23] K.P. Ng, T.A. Pascoal, S. Mathotaarachchi, et al., Monoamine oxidase B inhibitor, selegiline, reduces 18F-THK5351 uptake in the human brain, Alzheimers Res. Ther. 9 (2017) 25, https://doi.org/10.1186/s13195-017-0253-y.
[24] K. Zhu, X. Wang, B. Sun, et al., Primary age-related tauopathy in human subcortical nuclei, Front. Neurosci. 13 (2019) 529, https://doi.org/10.3389/fnins.2019.00529.
[25] J.S. Fowler, N.D. Volkow, G.J. Wang, et al., Age-related increases in brain monoamine oxidase B in living healthy human subjects, Neurobiol. Aging 18 (4) (1997) 431–435, https://doi.org/10.1016/s0197-4580(97)00037-7.
[26] J. Saura, Z. Bleuel, J. Ulrich, et al., Molecular neuroanatomy of human monoamine oxidases A and B revealed by quantitative enzyme radioautography and in situ hybridization histochemistry, Neuroscience 70 (3) (1996) 755–774, https://doi.org/10.1016/s0306-4522(96)83013-2.
[27] G. Cohen, Monoamine oxidase and oxidative stress at dopaminergic synapses, J. Neural Transm. Suppl. 32 (1990) 229–238, https://doi.org/10.1007/978-3-7091-9113-2_33.
[28] K.M. Park, H.J. Lee, B.I. Lee, et al., Alterations of the brain network in idiopathic rapid eye movement sleep behavior disorder: structural connectivity analysis, Sleep Breath. 23 (2) (2019) 587–593, https://doi.org/10.1007/s11325-018-1737-0.
[29] B. Deweer, S. Lehéricy, B. Pillon, et al., Memory disorders in probable Alzheimer's disease: the role of hippocampal atrophy as shown with MRI, J. Neurol. Neurosurg. Psychiatry 58 (5) (1995) 590–597, https://doi.org/10.1136/jnnp.58.5.590.
[30] A. Brück, R. Portin, A. Lindell, et al., Positron emission tomography shows that impaired frontal lobe functioning in Parkinson's disease is related to dopaminergic hypofunction in the caudate nucleus, Neurosci. Lett. 311 (2) (2001) 81–84, https://doi.org/10.1016/s0304-3940(01)02124-3.
[31] L.H. Hicks, J.E. Birren, Aging, brain damage, and psychomotor slowing, Psychol. Bull. 74 (6) (1970) 377–396, https://doi.org/10.1037/h0033064.
[32] P.D. Bruen, W.J. McGeown, M.F. Shanks, et al., Neuroanatomical correlates of neuropsychiatric symptoms in Alzheimer's disease, Brain 131 (9) (2008) 2455–2463, https://doi.org/10.1093/brain/awn151.
[33] J.W. van Dalen, L.L. van Wanrooij, E.P.M. van Charante, et al., Association of apathy with risk of incident dementia: a systematic review and meta-analysis, JAMA Psychiatry 75 (10) (2018) 1012–1021, https://doi.org/10.1001/jamapsychiatry.2018.1877.
[34] T.L. Jernigan, S.L. Archibald, C. Fennema-Notestine, et al., Effects of age on tissues and regions of the cerebrum and cerebellum, Neurobiol. Aging 22 (4) (2001) 581–594, https://doi.org/10.1016/s0197-4580(01)00217-2.
[35] N. Raz, K.M. Rodrigue, K.M. Kennedy, et al., Differential aging of the human striatum: longitudinal evidence, AJNR Am. J. Neuroradiol. 24 (9) (2003) 1849–1856.
[36] R. Eggers, H. Haug, D. Fischer, Preliminary report on macroscopic age changes in the human prosencephalon: a stereologic investigation, J. Hirnforsch. 25 (2) (1984) 129–139.